Simulation of Near-Surface Mesocyclogenesis during Mergers between Mature and Nascent Supercells

RYAN M. HASTINGS*

Department of Earth, Atmospheric, and Planetary Sciences, Purdue University, West Lafayette, Indiana

YVETTE P. RICHARDSON AND PAUL M. MARKOWSKI
Department of Meteorology, The Pennsylvania State University, University Park, Pennsylvania

ABSTRACT

Prior simulations of mergers between mature and nascent supercells show that during or following certain types of mergers, an intensification in the near-surface vertical vorticity field occurs. This intensification is similar to observations of certain real-world mergers. In order to investigate this further, trajectory and circulation analyses of the simulated mergers are employed to determine the processes responsible for the rapid intensification of low-level vorticity in interactions involving the merging of a nascent supercell into the rear flank of a mature supercell.

1. Introduction

Observational studies provide some evidence for a connection between mergers involving supercells and subsequent tornadogenesis (e.g., Lee et al. 2006; Wurman et al. 2007; Rogers and Weiss 2008; Rogers 2012). Lee et al. (2006) show a nearly Gaussian distribution of tornadogenesis events with respect to the initiation of merger (defined as the first overlap of the 30 dBZ logarithmic reflectivity factor contour at the lowest scanning angle), with more than half of the tornadoes beginning within five minutes of the initiation time of the merger. Rogers and Weiss (2008) and Rogers (2012) performed a similar study over one and five storm seasons, respectively, and found a similarly Gaussian distribution, with a slight preference for tornadogenesis during mergers in which an ancillary, ordinary cell merged into the southwest sector of a supercell. In addition, Wurman et al. (2007) sampled a supercell with mobile X-band Doppler radars as it underwent multiple mergers, with a brief tornado being produced during each merger. In addition to the observational evidence, some numerical studies have shown intensification of near-surface vorticity occurring during or after mergers (Jewett et al. 2006; Hastings and Richardson 2010; Syrowski et al. 2012; Hastings et al. 2012).

At the outset, it is helpful to define "merger." A variety of definitions have been used in the literature on convective cloud mergers, including the overlap of rain or cloud water mixing ratios, updraft contours, and rainfall rates (Westcott 1984). Because we want this work to be of service to operational meteorologists, we follow Lee et al. 2006 and adopt a definition based on radar reflectivity: *A merger occurs when two originally separate reflectivity maxima join at a reflectivity contour that is high relative to the original maxima, such that separate maxima no longer remain.*

Hastings et al. (2012) and Hastings (2013) performed a series of simulations of mergers between nascent and mature supercells, varying the timing and location of the interaction. They found that mergers can be classified into five categories that generally depend on the minimum separation between the updrafts. Low-level vortex intensification occurred in many of the experiments; however, the mechanisms of vortexgenesis were not examined in those studies. In particular, interactions during which the nascent supercell merged into the rear flank of the mature supercell were found to produce intense vortices following the merger, somewhat consistent with the findings of Rogers and Weiss (2008) and Rogers (2012). It is these rear-flank mergers that are examined herein. Section 2 describes the methodology of this study, Section 3 presents the results, and Section 4 provides some discussion of the results.

2. Methodology

The setup of the numerical experiments is identical to that described in Hastings et al. (2012). Convection in a numerical model is initiated at $t = 0$ s with a warm bubble having a maximum temperature excess of 2 K, with a

*Corresponding author address: Ryan M. Hastings, Department of Earth, Atmospheric, and Planetary Sciences, Purdue University, 550 Stadium Mall Dr., West Lafayette, IN 47907
E-mail: hastingr@purdue.edu

second warm bubble introduced at $t = 3300$ s. By varying the position of the second warm bubble, the maturity of the second storm and the location into which the second storm merged into the original storm could be controlled.

The model that was used is CM1r16 (Bryan and Fritsch 2002). The base state thermodynamic profile is the analytic sounding from Weisman and Klemp (1984). The hodograph has a semicircular shape with 17.5 m s^{-1} westerlies at the surface, the same magnitude of southerlies at $z = 2.5$ km, and easterlies at $z = 5$ km (Fig. 1). Winds are constant above $z = 5$ km. In the interest of identifying mechanisms inherent to the merger process itself, the numerical experiments are kept as idealized and as close to previous idealized studies of isolated supercells as possible. No surface physics, terrain, or radiation are included, and the vertical boundaries are rigid while the lateral boundaries are open-radiative (Orlanski 1976). The domain is 120×120×18.375 km. The horizontal grid spacing is 500 m, and the vertical grid stretches from 50 m at the lowest grid level to 700 m at the highest according to the analytic functions given in Anthes (1970). A Rayleigh sponge layer starts at $z = 14$ km. Subgrid turbulence is parameterized by the 1.5-order TKE scheme . The main departure from previous idealized studies is the use of the double-moment Morrison microphysics scheme (Morrison et al. 2005).

The model results were investigated using circulation analysis. According to Bjerknes' theorem, the change in circulation around a material circuit in inviscid flow is determined by the buoyancy forcing around the circuit according to

$$\frac{dC}{dt} = \oint B\,dz, \tag{1}$$

where B is the buoyancy and C is the circulation, defined by

$$C = \oint \mathbf{u} \cdot d\mathbf{l} = \int \boldsymbol{\omega} \cdot d\mathbf{A}, \tag{2}$$

with $\mathbf{u}$ as the wind, $d\mathbf{l}$ as an infinitesimal length along the circuit, $\boldsymbol{\omega}$ the vorticity, and $d\mathbf{A}$ the vector normal to an infinitesimal area dA defined by the circuit. Material circuits surrounding vorticity maxima were selected, and the trajectories of parcels within those material circuits were calculated backwards in order to determine the evolution of circulation along the circuts. Trajectories were calculated using a 4th-order Runge-Kutta scheme, using model data at every time step (3 s) in order to minimize trajectory errors associated with highly convergent or rotational flow (Dahl et al. 2012). The parcels in the initial circuit were placed approximately 190 m from each other in a 1.5-km-radius ring centered on the vorticity maximum at the lowest scalar grid level ($z = 25$ m). As the circuit evolved, a new parcel was introduced between any two parcels separated by more than 1 km. All of the interpolations used in this study were linear.

3. Results

Of the twelve simulations that are rear-flank mergers, all of them produced intense vortices at the lowest scalar grid level ($z = 25$ m) about 30 minutes after the initiation of merger. The vorticity maxima in these vortices were consistently two to three times stronger than the low-level vorticity maximum of a control run in which no second storm is introduced. For this section, we will focus on one particular model run, designated 15kmS15kmW in the Hastings (2013) study (Fig.2). The merger begins at 90 ($T+0$) minutes. The combined precipitation from both updrafts results in an outflow surge owing to the increased evaporative cooling and hydrometeor drag. By 120 ($T+30$) minutes, the system has transformed into a high-precipitation (HP) supercell. The mechanism of increased precipitation followed by a cold pool surge is similar to that identified in a simulation of an HP supercell undergoing multiple mergers by Finley et al. (2002).

A mesocyclone-strength (i.e., > 0.01 s^{-1}) vorticity maximum first appears at the lowest grid level around 120 ($T+30$) minutes. By 130 ($T+40$) minutes, two low-level mesocyclone-strength vorticity maxima can be seen along the gust front, with the northern maximum reaching nearly 0.06 s^{-1} (Fig. 3). In contrast, the vorticity maximum of the control storm at the same time is below 0.03 s^{-1}. Moreover, the post-merger storm shows greater circulation surrounding its vorticity maxima than the control storm (Fig. 4).

One of the principal differences relevant to the production of vorticity between the post-merger and control storm is in the strength of their cold pools as defined by Rotunno et al. (1998). Figure 5 shows that while the forward flanks have a comparable cold pool strength, the rear flanks differ, with the post-merger storm showing cold pool strength in excess of 30 m s^{-1} while the cold pool strength in the rear flank of the control storm does not exceed 20 m s^{-1}.

To begin exploring the influence of cold pool differences between the two storms, we compute the time tendency of circulation. For both the post-merger and the control storm, a material circuit with a 3-km diameter centered on the vorticity maximum was selected, and the trajectories computed backwards in time. The difference between the two storms is dramatic (Fig. 6). Circulation around the material circuit increases from just below $-2{\cdot}10^4$ m^2 s^{-1} to $6{\cdot}10^4$ m^2 s^{-1} for the post-merger storm, while that for the control storm varies between 2 and $4{\cdot}10^4$ m^2 s^{-1}. This shows that the circulation does increase, as a result of baroclinic processes along the path of the circuit.

4. Discussion

Circulation analysis suggests that the increased vorticity found following rear-flank mergers may be baroclinically produced. Comparing the cold pool strengths of

the two storms shows the main difference in the cold pool strengths between post-merger and control storms is in the rear flank. Further studies using parcel trajectories will be required to determine if this, in fact, is where the baroclinic generation of horizontal vorticity subsequently tilted and stretched into the vertical is occurring. Other areas of baroclinity, or other processes entirely, could play a role. Preliminary investigations of parcel trajectories show that most of the parcels entering the low-level mesocyclone descend from aloft after encountering the forward-flank downdraft, which also tends to be more negatively buoyant in post-merger HP supercells. Whether or not this has an impact, and if so what kind of impact, remains to be seen. In addition, these preliminary investigations suggest differences in the stretching of vertical vorticity in the final five minutes may play a significant role in the strength of the final vortex, with the post-merger storm showing stronger stretching than the control storm.

One question left untouched by this study, that will be the subject of future work, is the effect of merger on a pre-existing circulation. None of the storms simulated in Hastings et al. (2012) and Hastings (2013) had low-level mesocyclones at the time of merger. The impact of storm merger on already existing low-level mesocyclones constitutes an interesting problem.

Acknowledgments. The authors would like to acknowledge a number of people for helpful discussions relating to this work: George Bryan, Johannes Dahl, Daniel Dawson, David Dowell, Cathy Finley, Adam French, Alicia Klees, Bruce Lee, Jim Marquis, Hugh Morrison, Chris Nowotarski, Jaret Rogers, Robin Tanamachi, Hans Verlinde, Fred Wolf, and Joshua Wurman. This work was supported by National Science Foundation grant AGS-1157646.

REFERENCES

Anthes, R. A., 1970: Numerical experimenting with a two-dimensional horizontal variable grid. *Mon. Wea. Rev.*, **98**, 810–822.

Bryan, G. H., and J. M. Fritsch, 2002: A benchmark simulation for moist nonhydrostatic numerical models. *Mon. Wea. Rev.*, **130**, 2917–2928.

Dahl, J. M. L., M. D. Parker, and L. J. Wicker, 2012: Uncertainties of trajectory calculations within near-surface mesocyclones of simulated supercells. *Mon. Wea. Rev.*, **140**, 2959–2966.

Hastings, R. M., 2013: Long-term morphological changes in mature supercells following mergers with nascent cells in environments with directionally-varying shear. Ph.D. dissertation, The Pennsylvania State University, 155 pp.

_____ and Y. P. Richardson, 2010: Storm mergers. Part I: Preliminary numerical investigations of merger events. *25th Conf. on Severe Local Storms*, Denver, CO, 7A.5.

_____, _____, P. M. Markowski, J. M. Wurman and C. C. Weiss, 2012: Mergers in supercell environments. Part I: Conceptual models of mechanisms governing merger outcomes. *26th Conf. on Severe Local Storms*, Nashville, TN, 11B.6.

Jewett B. F., R. W. Przybylinsky, and R. B. Wilhelmson, 2006: Numerical simulation of the 24 April, 2002 storm merger between a left moving storm and supercell. Preprints, *23rd Conference on Severe Local Storms*, St. Louis, MO, Amer. Meteor. Soc., P11.3.

Lee, B. D., B. F. Jewett and R. B. Wilhelmson, 2006: The 19 April 1996 Illinois tornado outbreak. Part II: Cell mergers and associated tornado incidence. *Wea. Forecasting*, **21**, 449–464.

Morrison, H., Curry, J. A., and V. I. Khvorostyanov, 2005: A new double-moment microphysics parameterization for application in cloud and climate models. Part I: Description. *J. Atmos. Sci.*, **62**, 1665–1677.

Orlanski, I., 1976: A simple boundary condition for unbounded hyperbolic flows. *J. Comp. Sci.*, **21**, 251–269.

Rogers, J. W., 2012: Significant tornado events associated with cell mergers. *26th Conf. on Severe Local Storms*, Nashville, TN, 9.4.

_____, and C. C. Weiss, 2008: The association of cell mergers with tornado occurrence. *24th Conf. on Severe Local Storms*, Savannah, GA, P3.23.

Syrowski, A., B. F. Jewett and R. B. Wilhelmson, 2012: An assessment of internal and external forcings in supercell interactions and their impact on storm morphology. *26th Conf. on Severe Local Storms*, Nashville, TN 11B.5.

Weisman, M. L. and J. B. Klemp, 1984: The structure and classification of numerically simulated convective storms in directionally varying wind shears. *Mon. Wea. Rev.*, **112**, 2479–2498.

Westcott, N., 1984: A historical perspective on cloud mergers. *Bull. Amer. Meteor. Soc.*, **65**, 219–226.

Wurman, J. M., Y. P. Richardson, C. Alexander, S. Weygandt, and P. F. Zhang, 2007: Dual-Doppler and single-Doppler analysis of a tornadic storm undergoing mergers and repeated tornadogenesis. *Mon. Wea. Rev.*, **135**, 736–758.

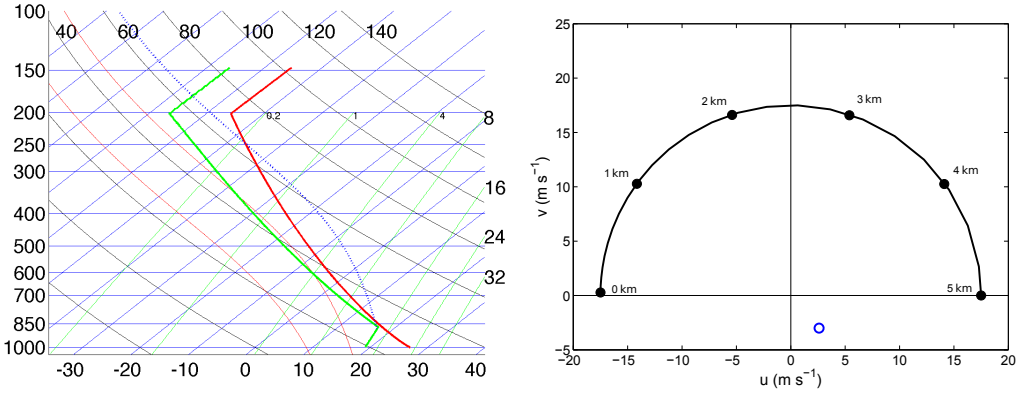

FIG. 1. Skew-T log-p diagram (left) and hodograph (right) for base state. Blue circle on hodograph indicates storm motion.

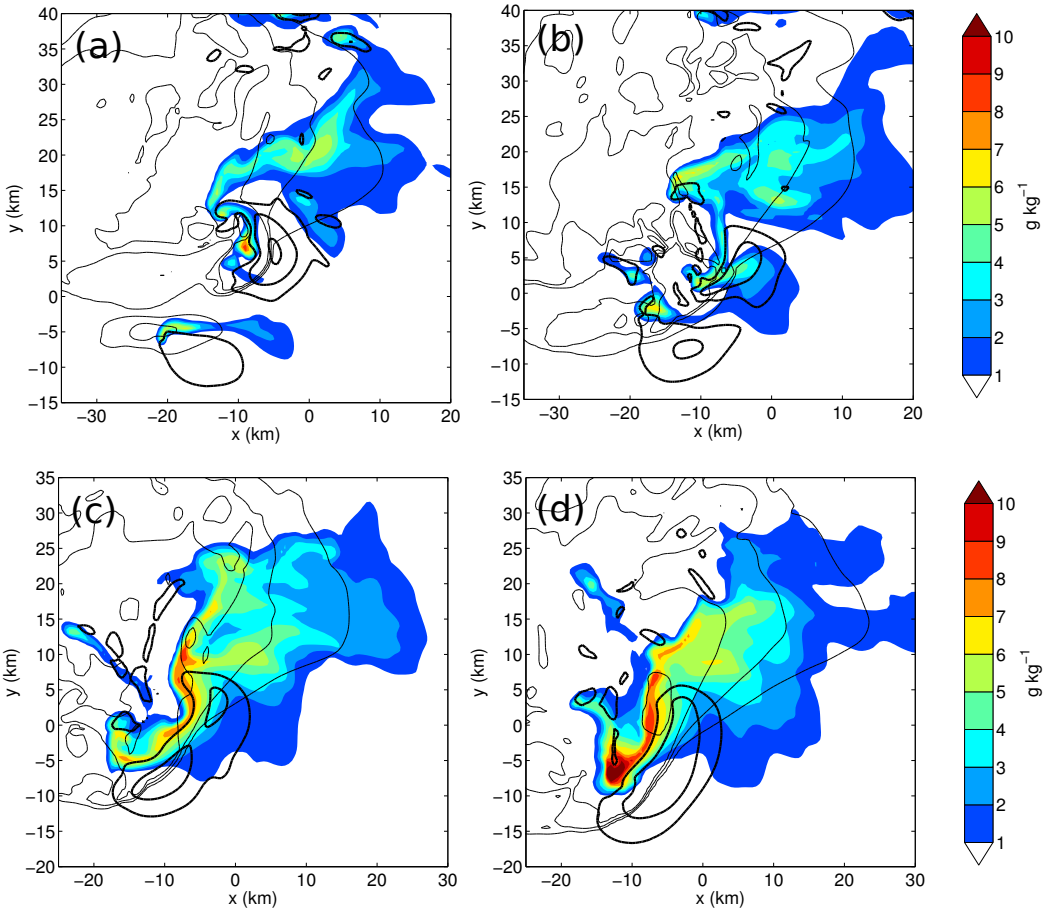

FIG. 2. 2.5 km precipitation mixing ratio shaded, updraft contoured in thick black every 10 m s^{-1} starting at 5 m s^{-1}, 25 m density potential temperature perturbation contoured in thin black at -1, -3, and -5 K. (a) 90 ($T+0$) min. (b) 100 ($T+10$) min. (c) 110 ($T+20$) min. (d) 120 ($T+30$) min.

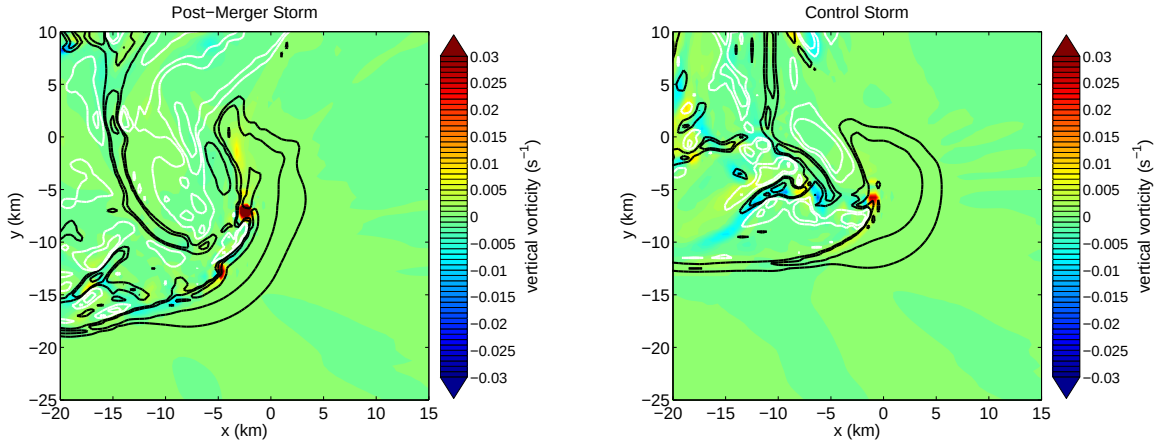

FIG. 3. 25 m vertical vorticity shaded, upward (downward) vertical velocity contoured in black (white) at 0.1, 0.2 and 0.5 (-0.5, -0.2, -0.1) m s^{-1} at 130 minutes for post-merger storm (left) and control storm (right).

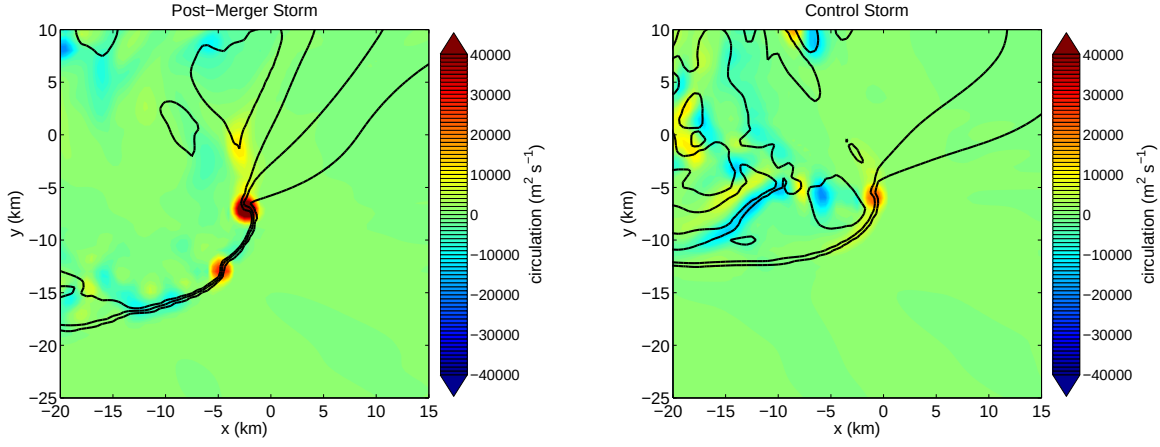

FIG. 4. 25 m circulation around a 1-km ring centered at each point shaded, density potential temperature perturbation contoured at -5, -3 and -1 K at 130 minutes for post-merger storm (left) and control storm (right).

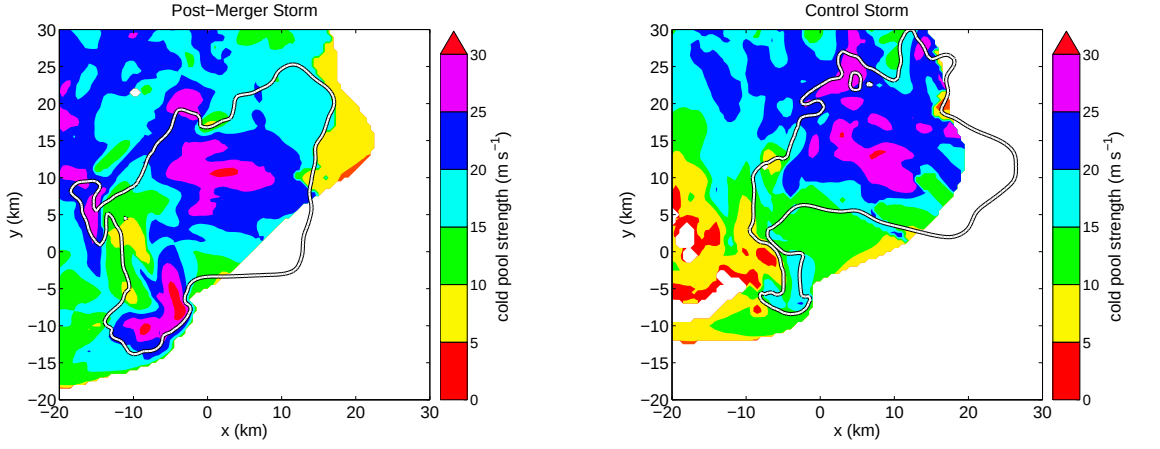

FIG. 5. Cold pool strength shaded, 1 km 1 g kg^{-1} precipitation mixing ratio contoured at 130 minutes for post-merger storm (left) and control storm (right).

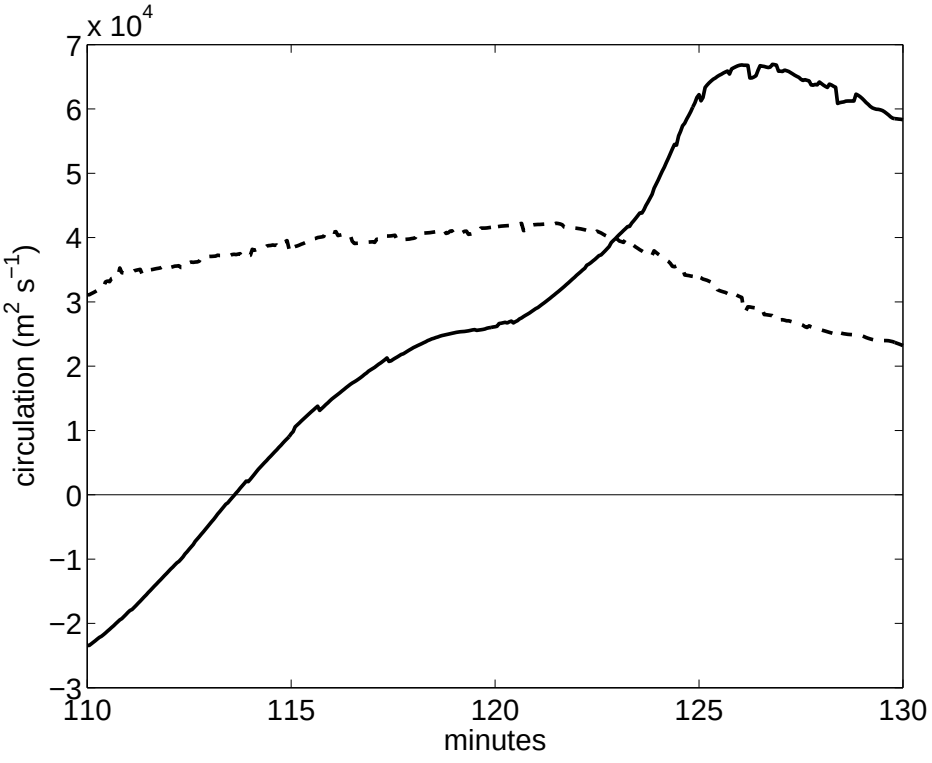

FIG. 6. Comparison of circulation for post-merger (solid) and control (dashed) storms.